THE JOURNAL OF BIOLOGICAL CHEMISTRY VOL. 282, NO. 11, pp. 8265–8275, March 16, 2007

Both the N-terminal Loop and Wing W2 of the Forkhead Domain of Transcription Factor Foxo4 Are Important for DNA Binding*

Received for publication, June 14, 2006, and in revised form, January 8, 2007 Published, JBC Papers in Press, January 23, 2007, DOI 10.1074/jbc.M605682200

Evzen Boura[‡§], Jan Silhan[‡§], Petr Herman[¶], Jaroslav Vecer[¶], Miroslav Sulc[‖], Jan Teisinger[§], Veronika Obsilova[§], and Tomas Obsil[‡§1]**

*From the Departments of [‡]Physical and Macromolecular Chemistry and [‖]Biochemistry, Faculty of Science, Charles University, 12843 Prague, the [¶]Faculty of Mathematics and Physics, Institute of Physics, Charles University, 12116 Prague, and the Institutes of [§]Physiology and **Microbiology, Academy of Sciences of the Czech Republic, 14220 Prague, Czech Republic*

FoxO4 belongs to the "O" subset of forkhead transcription factors, which participate in various cellular processes. The forkhead DNA binding domain (DBD) consists of three-helix bundle resting on a small antiparallel β-sheet from which two extended loops protrude and create two wing-like structures. The wing W2 of FoxO factors contains a 14-3-3 protein-binding motif that is phosphorylated by protein kinase B in response to insulin or growth factors. In this report, we investigated the role of the N-terminal loop (portion located upstream of first helix H1) and the C-terminal region (loop known as wing W2) of the forkhead domain of transcription factor FoxO4 in DNA binding. Although the deletion of either portion partly reduces the FoxO4-DBD binding to the DNA, the simultaneous deletion of both regions inhibits DNA binding significantly. Förster resonance energy transfer measurements and molecular dynamics simulations suggest that both studied N- and C-terminal regions of FoxO4-DBD directly interact with DNA. In the presence of the N-terminal loop the protein kinase B-induced phosphorylation of wing W2 by itself has negligible effect on DNA binding. On the other hand, in the absence of this loop the phosphorylation of wing W2 significantly inhibits the FoxO4-DBD binding to the DNA. The binding of the 14-3-3 protein efficiently reduces DNA-binding potential of phosphorylated FoxO4-DBD regardless of the presence of the N-terminal loop. Our results show that both N- and C-terminal regions of forkhead domain are important for stability of the FoxO4-DBD·DNA complex.

The winged helix or forkhead box (Fox)[2] transcription factors are a family of structurally related transcriptional activators involved in embryogenesis, tumorigenesis, and the metabolism control (1–4). Members of this family share a conserved 100-amino acid large DNA binding domain (DBD) containing three α-helices, three β-strands, and two wing-like loops (see Fig. 1*A*) (5–11). The highest degree of sequence conservation among DBD is found in three helices, H1, H2, and H3. Co-crystal structure of transcription factor HNF-3γ showed 14 protein-DNA contacts distributed throughout the forkhead domain (5). The main DNA recognition site is α-helix H3, which makes contacts with the major groove of DNA. Other regions of forkhead domain that can make important interactions with DNA are both wings (5) or N-terminal extension upstream of helix H1 (12). Structural studies have shown that binding to the DNA causes only small structural changes in the DBD but induces significant bending of the target DNA (10, 13). The molecular mechanism of Fox factors binding specificity for target DNA is still poorly understood. Because various forkhead proteins belonging to different subgroups share almost identical folds the variations in DBD topology cannot explain distinct DNA-binding specificities. Therefore other features of forkhead proteins, *e.g.* differences in charge distribution in the DNA binding interface, are likely to be responsible for DNA-binding specificities (9, 14).

Within the large family of Fox transcription factors, the proteins FoxO1 (FKHR), FoxO3a (FKHR-L1), FoxO4 (AFX), and FoxO6 constitute the "O" subfamily. Members of this subfamily play an important role in cellular proliferation, survival, and in mediating effects of insulin and growth factors on metabolism (15–17). All FoxO proteins function under the control of the phosphoinositide 3-kinase-protein kinase B (PKB) pathway. Phosphorylation by PKB creates two binding sites for the 14-3-3 protein and induces phosphorylation of additional sites by casein kinase 1 and dual-specificity tyrosine-regulated kinase 1A (18–21). PKB-mediated phosphorylation induces binding of the 14-3-3 protein, and the resulting complex is then translocated to the cytosol where the bound 14-3-3 protein prevents re-entry of FoxO into the nucleus likely by masking its nuclear localization sequence (18, 22–27).

* This work was supported by the Grant Agency of the Czech Republic (Grant 204/06/0565), by the Grant Agency of the Academy of Sciences of the Czech Republic (Grant KJB500110601), by the Ministry of Education, Youth, and Sports of the Czech Republic (Research Projects MSM0021620857, MSM0021620835, and Centre of Neurosciences LC554), and by of the Academy of Sciences of the Czech Republic (Research Project AV0Z50110509). The costs of publication of this article were defrayed in part by the payment of page charges. This article must therefore be hereby marked "*advertisement*" in accordance with 18 U.S.C. Section 1734 solely to indicate this fact.

[1] To whom correspondence should be addressed. Tel.: 420-221-951-303; Fax: 420-224-919-752; E-mail: obsil@natur.cuni.cz.

[2] The abbreviations used are: Fox, forkhead box; 1,5-IAEDANS, 5-((((2-iodoacetyl)amino)ethyl)amino)naphthalene 1-sulfonic acid; AEDANS, 5-(((acetylamino)ethyl)amino)naphthalene 1-sulfonic acid; DBD, DNA binding domain; MALDI-TOF, matrix-assisted laser desorption ionization time-of-flight; MD, molecular dynamics; FoxO4-DBD, DNA binding domain of FoxO4 fragment 82–207; $pFoxO4_{82–207}$, phosphorylated $FoxO4_{82–207}$; $dpFoxO4_{11–213}$, doubly phosphorylated $FoxO4_{11–213}$; PKB, protein kinase B; r.m.s.d., root mean square deviation; WT, wild type; DTT, dithiothreitol; FLC, fluorescein; FRET, fluorescence resonance energy transfer.

The DNA-binding potential of FoxO-DBD is controlled by multiple mechanisms. The most important factors seem to be the PKB-induced phosphorylation and the binding of the 14-3-3 protein (22–24, 28). The PKB phosphorylation site and the 14-3-3 protein-binding motif are located in the basic region of wing W2 at the C terminus of FoxO-DBD (Fig. 1*B*). Structures of HNF-3γ (FoxA3) and Genesis (FoxD3) complexes revealed that the cluster of basic residues in the wing W2 is involved in DNA binding (5, 10). Moreover, the removal of wing W2 abolishes DNA binding of forkhead transcription factor HNF-3α (29). Sequence alignment between HNF-3γ, Genesis, and FoxO sequences suggests that analogue-basic residues forming the second FoxO PKB phosphorylation site and the 14-3-3 binding motif might participate in DNA binding as well (Fig. 1*B*). This similarity could explain the inhibitory effect of both the phosphorylation and the 14-3-3 protein on DNA-binding activity of FoxO proteins. However, the regulation of DNA binding among various FoxO proteins seems to differ significantly. It has been shown that the phosphorylation of the second PKB/14-3-3 binding motif in the wing W2 suppresses DNA binding of FoxO1 and FoxO6 factors (28, 30). On the other hand, the PKB-induced phosphorylation of both DAF-16 (*Caenorhabditis elegans* FoxO homologue) and FoxO4 (fragment 11–213) does not by itself affect their binding to the target DNA (22, 23). Binding of the 14-3-3 protein to phosphorylated FoxO4 and DAF-16 has been shown to be necessary for complete inhibition of their binding to the DNA.

To better understand these differences among FoxO-DBD, we investigated the role of N-terminal loop (portion located upstream of the first helix H1) and C-terminal region (loop known as wing W2) of forkhead domain of transcription factor FoxO4 in DNA binding. Although the deletion of either the N- or C-terminal portion of forkhead domain partly reduces the FoxO4-DBD binding to the DNA, the simultaneous deletion of both regions inhibits DNA binding significantly. Förster resonance energy transfer measurements and molecular dynamics simulations suggest that both N- and C-terminal regions of FoxO4-DBD studied directly interact with the DNA. In the presence of N-terminal part the PKB-induced phosphorylation of wing W2 by itself has negligible effect on DNA binding. On the other hand, in the absence of this loop the phosphorylation of wing W2 significantly inhibits the FoxO4-DBD binding to the DNA. The binding of the 14-3-3 protein efficiently reduces DNA-binding potential of phosphorylated FoxO4-DBD regardless of the presence of N-terminal region. Our results show that both N- and C-terminal regions of forkhead domain are important for the stability of FoxO4-DBD·DNA complex.

EXPERIMENTAL PROCEDURES

Expression, Purification, and Phosphorylation of FoxO4-DBD—Expression plasmid for FoxO4-DBD ($FoxO4_{82-207}$) was a kind gift of Dr. J. Weigelt. FoxO4-DBD mutants containing a single Cys residue at two different positions in the wing W2 (mutation $Ser^{183} \rightarrow Cys$ and $Ser^{193} \rightarrow Cys$) were generated using the QuikChange kit (Stratagene). To generate C-terminally truncated FoxO4-DBDΔC ($FoxO4_{82-183}$) a stop codon was introduced instead of Gly^{184}. To create N-terminally truncated FoxO4-DBDΔN the DNA-encoding sequence $FoxO4_{98-199}$ was ligated into pET-15b (Novagen) using the NdeI site. To generate doubly truncated FoxO4-DBDΔNΔC, a stop codon was introduced into a DNA of FoxO4-DBDΔN at position 184. All mutations were confirmed by sequencing. All versions and mutants of FoxO4-DBD have been expressed and purified as described previously (9). Briefly, FoxO4-DBD was expressed as 6×His tag fusion proteins by isopropyl 1-thio-β-D-galactopyranoside induction for 12 h at 30 °C and purified from *Escherichia coli* BL21(DE3) cells using Chelating-Sepharose Fast Flow (Amersham Biosciences) according to the standard protocol. Eluted protein was dialyzed against buffer 50 mM sodium citrate (pH 6.3), 2 mM EDTA, 1 mM DTT and purified using cation-exchange chromatography on an SP-Sepharose column (Amersham Biosciences). The protein was eluted using linear gradient of NaCl (50–1000 mM). Fractions containing FoxO4-DBD were dialyzed against buffer containing 20 mM Tris (pH 7.5), 50 mM NaCl, 1 mM EDTA, 2 mM DTT, and 10% (v/w) glycerol. Purified FoxO4-DBD was then phosphorylated by incubation with 9 units of PKBα (Upstate Biotechnology) per milligram of recombinant protein for 2 h at 30 °C in the presence of 10 mM magnesium acetate and 0.2 mM ATP. After the phosphorylation, the FoxO4-DBD was re-purified using cation-exchange chromatography as mentioned above. Eluted proteins were finally dialyzed against buffer containing 20 mM Tris (pH 7.5), 50 mM NaCl, 1 mM EDTA, 2 mM DTT, and 10% (w/v) glycerol. The completeness of the phosphorylation reaction was checked using the MALDI-TOF mass spectrometry.

Mass Spectrometric Analysis of FoxO4-DBD—Samples were first separated by 15% SDS-PAGE, and excised protein bands were digested with Lys-C endoprotease (Promega, Madison, WI) directly in gel (31). Resulting peptide mixtures were extracted by 30% acetonitrile and 0.3% acetic acid and subjected to MALDI-TOF mass spectrometer BIFLEX (Bruker-Franzen, Bremen, Germany) equipped with a nitrogen laser (337 nm) and gridless delayed extraction ion source. Ion acceleration voltage was 19 kV, and the reflectron voltage was set to 20 kV. Spectra were calibrated externally using the monoisotopic $[M+H]^+$ ion of FoxO4 peptides with known sequence. A saturated solution of α-cyano-4-hydroxycinnamic acid in 50% MeCN/0.3% acetic acid was used as the MALDI matrix. 1 μl of the sample was loaded on the target, and the droplet was allowed to dry at ambient temperature, overlaid with 1 μl of matrix solution, and allowed to co-crystallize also at ambient temperature.

Labeling of FoxO4-DBD Mutants by 1,5-IAEDANS—The Forkhead domain of FoxO4 (fragment 82–207) does not contain any cysteine residue. To prepare FoxO4-DBD specifically labeled with fluorescence probe at two different position in the wing W2 we inserted a single Cys residue at positions 183 (mutation $Ser^{183} \rightarrow Cys$) and 193 (mutation $Ser^{193} \rightarrow Cys$). Covalent modification of FoxO4-DBD containing single cysteine residue with thiol-reactive probe 1,5-IAEDANS was carried out as described elsewhere (32). Briefly, the protein (50–70 μM) in 50 mM Tris (pH 7.5), 100 mM NaCl, 1 mM EDTA and label were mixed at a molar ratio of 1:40 and incubated at 30 °C for 2 h, and then at 4 °C overnight in the dark. The free unreacted label was removed by gel filtration in buffer containing 50 mM Tris (pH 7.5), 100 mM NaCl, and 1 mM EDTA. The incor-

poration stoichiometry was determined by comparing the peak protein absorbance at 280 nm with the absorbance of bound 1.5-IAEDANS measured at 336 nm using an extinction coefficient of 5700 M^{-1} cm^{-1} (Molecular Probes, Eugene, OR).

Expression and Purification of 14-3-3 Protein—Human 14-3-3 protein (zeta isoform) was expressed and purified as described previously (33). Briefly, 14-3-3ζ was expressed as a 6×His tag fusion protein by isopropyl 1-thio-β-D-galactopyranoside induction for 12 h at 20 °C and purified from *E. coli* BL21(DE3) cells using Chelating-Sepharose. The histidine tag was removed by incubation for 6 h at 15 °C with 10 units of thrombin/mg of protein. After cleavage, 14-3-3 protein was purified using anion-exchange chromatography on a Q-Sepharose column (Amersham Biosciences). The protein was eluted using a 50–600 mM NaCl gradient in 50 mM Tris-HCl (pH 8.0) and 1 mM DTT and dialyzed overnight against buffer containing 20 mM Tris (pH 7.5), 100 mM NaCl, 1 mM EDTA, 5 mM DTT, and 10% (w/v) glycerol.

Steady-state Fluorescence Measurements—Fluorescence spectra were taken on a PerkinElmer Life Sciences LS50B spectrofluorometer at 22 °C with 0.6 μM protein and 0.6 μM dsDNA in 50 mM Tris-HCl (pH 7.5), 100 mM NaCl, and 1 mM EDTA in 10-mm cell. Excitation was done at 336 nm; the bandwidths were 5 nm for both excitation and emission. The following oligonucleotides containing consensus FoxO binding sequence were used to prepare samples of dsDNA: S1, 5′-GCGTTGTTTACGC-3′; S2, 5′-GCGTAAACAACGC-3′; fluorescein-labeled S1FLC, 5′-FLC-GCGTTGTTTACGC-3; and S2FLC, 5′-FLC-GCGTAAACAACGC-3′. Double-stranded DNA denoted as "S1FLC/S2" was prepared by mixing oligonucleotides S1FLC and S2; dsDNA denoted as "S1/S2FLC" was prepared by mixing oligonucleotides S1 and S2FLC.

Steady-state Fluorescence Anisotropy DNA Binding Measurements—Steady-state fluorescence measurements were performed on a PerkinElmer Life Sciences LS50B fluorescence spectrometer at 22 °C with 100 nM dsDNA labeled with fluorescein at the 5′ terminus of both strands (S1FLC/S2FLC). Increasing amounts of protein were titrated into the cuvette. At each FoxO4-DBD concentration, the steady-state fluorescence anisotropy of fluorescein was recorded (excitation at 494 nm and emission at 520 nm). Anisotropy was calculated from the fluorescence intensities according to the relationship, $r = (I_{II} - I_{\perp})/(I_{II} + 2I_{\perp})$. The fraction of DNA bound (F_B) was calculated from Equation 1,

$$F_B = (r_{obs} - r_{min})/[(r_{max} - r_{obs})Q + (r_{obs} - r_{min})] \quad \text{(Eq. 1)}$$

where Q represents the quantum yield ratio of the bound to the free form; it was estimated by calculating the ratio of the intensities of the bound to the free fluorophore. Parameter r_{max} is the anisotropy at saturation, r_{obs} is the observed anisotropy for any FoxO4-DBD concentration, and r_{min} is the minimum observed anisotropy of the free DNA. F_B was plotted against the FoxO4-DBD protein concentration and fitted using Equation 2 to determine the K_D for FoxO4-DBD·dsDNA complex formation (34),

$$F_B = \frac{K_D + [P_1] + [P_2] - \sqrt{(K_D + [P_1] + [P_2])^2 - 4[P_1][P_2]}}{2[P_1]} \quad \text{(Eq. 2)}$$

where K_D is the equilibrium dissociation constant, $[P_1]$ is the dsDNA-fluorescein concentration, and $[P_2]$ is the FoxO4-DBD concentration. Non-linear data fitting was performed using the Origin 6.0 package (MicroCal Software Inc.).

Time-resolved Fluorescence Measurements—Fluorescence resonance energy transfer was observed between the AEDANS moiety covalently attached to Cys^{183} or Cys^{193} of FoxO4-DBD and fluorescein (FLC) moiety attached to the 5′ terminus of one of the dsDNA strands. Fluorescence intensity decays were measured on the laser-based time-correlated single photon counting apparatus with multichannel plate photomultiple detection described in detail previously (35). Fluorescence decays have been acquired under the "magic angle" conditions when the measured intensity decay $I(t)$ is independent of a rotational diffusion of the chromophore and provides unbiased information about fluorescence lifetimes. The samples were placed in a thermostatic holder, and all experiments were performed at 15 °C in buffer containing 50 mM Tris-HCl (pH 7.5), 100 mM NaCl, and 1 mM EDTA. FoxO4-DBD concentration was 2.4 μM, and dsDNA concentration was 6 μM. Dansyl fluorescence was excited and collected at 315 and 370 nm, respectively. Fluorescence decays were processed using the singular value decomposition maximum entropy method, and mean lifetimes were calculated as described previously (35). The averaged efficiency of energy transfer E was calculated from the mean donor lifetime in the presence (τ_{DA}) and in the absence of acceptor (τ_D) in Equation 3.

$$E = 1 - (\tau_{DA}/\tau_D) \quad \text{(Eq. 3)}$$

The average distance between the donor-acceptor pair R was calculated from Equation 4,

$$R = R_0 \cdot \sqrt[6]{1/E - 1} \quad \text{(Eq. 4)}$$

where R_0 is the critical Förster distance (the distance at which the energy transfer occurs with 50% efficiency). An R_0 value of 49 Å determined for AEDANS and fluorescein pair was used to calculate R (36, 37).

Molecular Simulations—The MD simulations were performed using the GROMACS package 3.3 with the AMBER-94 parameter set exported to the GROMACS format (38). To prepare the starting structure the solution structure of FoxO4-DBD (sequence 92–181, PDB access code 1E17) was fitted onto the co-crystal structure of transcription factor HNF-3γ with bound DNA (5, 9). The missing wing W2 of FoxO4-DBD was modeled (up to residue 193) using the structures of transcription factors HNF-3 and Genesis as templates (5, 10). Coordinates of dsDNA (S1/S2) containing the consensus FoxO binding sequence (5′-GCGTTGTTTACGC-3′) were generated using the FIBER program from the 3DNA package (39). The molecule of dsDNA was oriented in such a way that the motif 5′-TGTTT-3′ was superimposed with the motifs 5′-TATTT-3′ from the solution structure of Genesis·DNA complex and 5′-

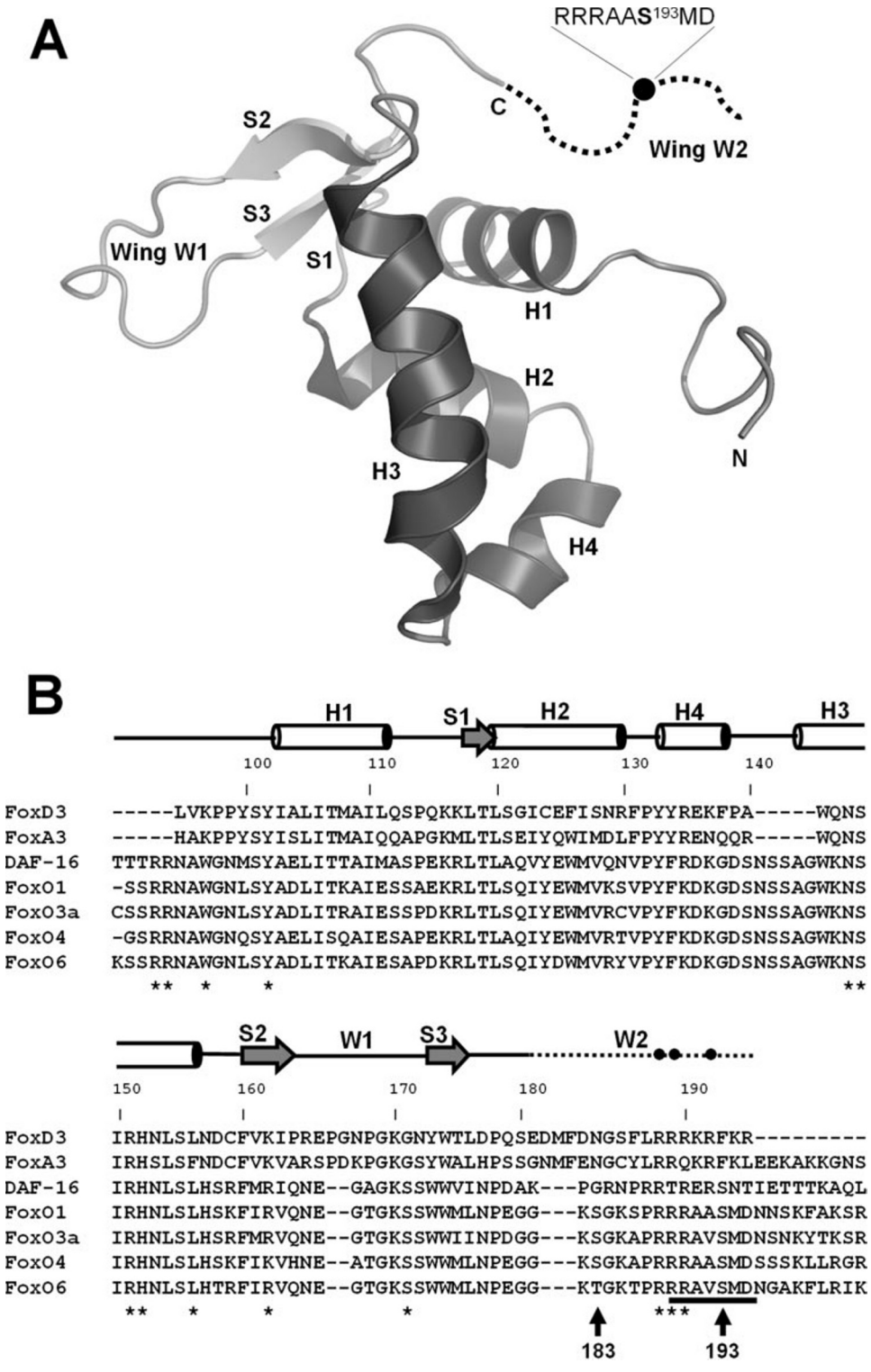

FIGURE 1. **Structure of FoxO4-DBD.** *A*, the *ribbon representation* of the solution structure of FoxO4-DBD sequence Ser^{92}–Gly^{181} (9). The missing part of wing W2 is schematically shown as a *dotted line*. The *black circle* represents the approximate location of the PKB phosphorylation site Ser^{193}. *B*, sequence alignment of the DNA binding domain from selected Forkhead box transcription factors: FoxD3/Genesis (*Rattus norvegicus*, SwissProt Q63245); FoxA3/HNF-3γ (*R. norvegicus*, SwissProt P32183); DAF-16 (*C. elegans*, SwissProt O18676); FoxO1 (*Homo sapiens*, SwissProt Q12778); FoxO3a (*H. sapiens*, SwissProt Q43524); FoxO4 (*H. sapiens*, SwissProt P98177); and FoxO6 (*Mus musculus*, SwissProt Q5RJI9). Secondary structure elements are indicated at the *top*. *Black circles* indicate basic residues from the wing W2 that interact with DNA (5, 10). *Arrows* indicate serine residues that were mutated to cysteines for the attachment of AEDANS moiety. *Underlined* FoxO4 sequence denotes 14-3-3 protein-binding motif. *Stars* indicate residues predicted by MD simulation to make contact with DNA.

GACTT-3′ from the crystal structure of HNF-3γ·DNA complex. FoxO4-DBD·DNA complex was then solvated with water in a periodic box using the TIP3P water model (40). All water molecules within 1.5 Å of any protein or DNA atom were removed. The system was electroneutralized by replacing water molecules with the highest electrostatic potential energy with Na^+ ions. Next, the resulting system was energy-minimized using the steepest descent method. This was followed by a 50-ps equilibration MD run during which position restraints were applied on the complex. The system was then set completely free, and an MD simulation 40 ns long at 300 K temperature and 1 bar pressure was performed. Simulation of FoxO4-DBD alone (20 ns long) was performed using the same protocol. Both simulations were run with a 2-fs time step. Solute, solvent, and counterions were independently weakly coupled to a reference temperature bath (41) with a coupling constant of $\tau_T = 0.1$ ps. The initial velocities were obtained from a Maxwellian distribution at the desired temperature. The pressure was controlled using the Berendsen algorithm with a coupling constant of $\tau_P = 0.5$ ps. All bond lengths were constrained using LINCS (42). The particle mesh Ewald method was used to treat electrostatic interactions (43). The cut-off for van der Waals interactions was set to 9 Å. Trajectories were analyzed using the GROMACS software package (44). Cluster analysis was performed using the GROMOS method (45).

RESULTS

Characterization of Phosphorylated FoxO4-DBD—In this report, we studied a human FoxO4-DBD (sequence 82–207) containing forkhead domain and one PKB phosphorylation site Ser^{193} located in the wing W2 (Fig. 1). FoxO4-DBD protein and its N-terminally truncated version FoxO4-DBDΔN were phosphorylated by PKB, and the result of phosphorylation reaction was determined using MALDI-TOF mass

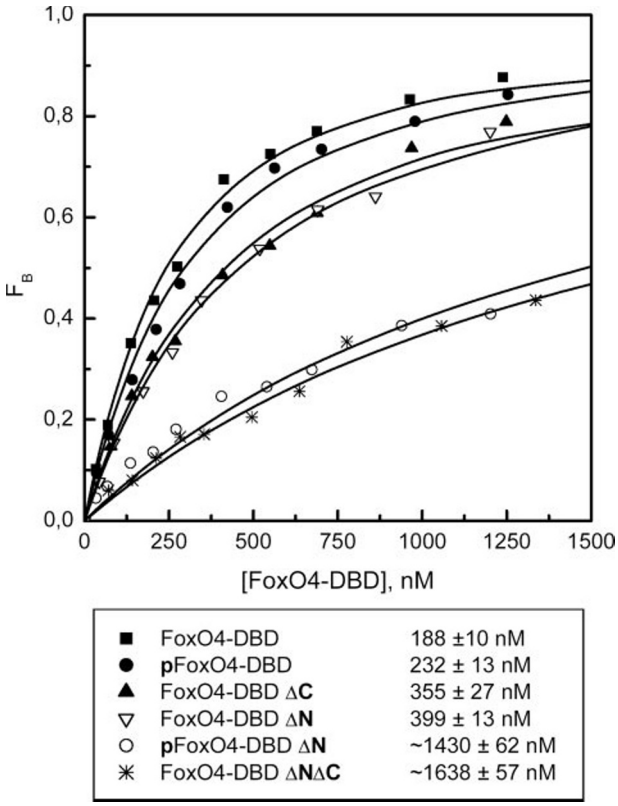

FIGURE 2. **Effect of phosphorylation and truncations on DNA-binding properties of FoxO4-DBD.** Fluorescence anisotropy binding assays were performed using a dsDNA probe labeled at the 5′-end of both strands with fluorescein. Binding studies were performed with unphosphorylated intact FoxO4-DBD, phosphorylated (at Ser^{193}) intact pFoxO4-DBD, C-terminally truncated FoxO4-DBDΔC, N-terminally truncated FoxO4-DBDΔN, phosphorylated (at Ser^{193}) N-terminally truncated pFoxO4-DBDΔN, and doubly truncated FoxO4-DBDΔNΔC.

spectrometry. Positive ion mass spectra were measured in the reflection mode to check the amino acid sequences of unphosphorylated and phosphorylated FoxO4-DBD tryptic peptides. The comparison of positive MALDI-TOF mass spectra of digested unphosphorylated and phosphorylated proteins clearly demonstrates the phosphorylated peptide of FoxO4-DBD. The detected peaks in positive ion mass spectra of phosphorylated pFoxO4-DBD having the protonized mass of 1599.6 (m/z) correspond to phosphorylated peptide APRRRAASMDSSSK (the PKB phosphorylation/14-3-3 protein-binding motif is ^{189}RRAAS^{193}) and the same peptide with oxidized methionine in its sequence having the mass of 1615.7 (m/z). On the other hand, the unphosphorylated protein mass spectrum provided no peaks with the same values of m/z there. The identity and structure of both phosphorylated peptides (with or without methionine oxidation) was further corroborated by analysis of their post source decay spectra to authenticate Ser^{193} as the phosphorylated amino acid (data not shown).

Effects of Truncations and Phosphorylation on DNA Binding Affinity of FoxO4-DBD—To assess the role of both N-terminal extension and C-terminal wing W2 in FoxO4-DBD binding to the DNA, we compared a DNA binding affinity of intact FoxO4-DBD and both N- and C-terminally truncated versions using the fluorescence anisotropy-based binding assay with a fluorescein-tagged dsDNA (Fig. 2). Intact FoxO4-DBD (sequence 82–207) binds to dsDNA with K_D of 188 ± 10 nM. The removal of wing W2 at the C terminus of forkhead domain caused a 2-fold increase in K_D to 355 ± 27 nM. A similar effect was also observed in the case of N-terminal truncation, where the removal of residues located upstream of helix H1 lead to a 2-fold increase in K_D to 399 ± 13 nM. Simultaneous deletion of both terminal portions, however, profoundly inhibited the DNA-binding potential of FoxO4-DBD ($K_D \sim 1638 \pm 57$ nM). Next, we studied the effect of PKB-induced phosphorylation of wing W2 at Ser^{193}. Phosphorylation of intact FoxO4-DBD induced only a minor change of DNA binding affinity (K_D = 232 ± 13 nM), whereas the phosphorylation of N-terminally truncated FoxO4-DBDΔN caused significant inhibition of DNA binding affinity ($K_D \sim 1430 \pm 62$ nM). These data indicate that both N- and C-terminal regions participate in DNA binding and probably stabilize the protein·DNA complex. In addition, it seems that phosphorylation at Ser^{193} by itself has negligible influence on DNA-binding properties of intact FoxO4-DBD, whereas phosphorylation of FoxO4-DBDΔN reduces the DNA binding affinity to the same extent as observed in the case of doubly truncated FoxO4-DBDΔNΔC.

14-3-3 Protein Binding to Wing W2 Inhibits DNA Binding Potential of FoxO4-DBD—Phosphorylation of FoxO proteins by PKB creates two 14-3-3 recognition motifs and induces the binding of 14-3-3 proteins to FoxO factors (18, 23, 24, 26). The exact role of the 14-3-3 protein in the regulation of FoxO transcription factors activity is still not fully understood. Interactions between 14-3-3 proteins and phosphorylated FoxO4 (fragment 11–213) or phosphorylated DAF-16 have been shown to result in inhibition of DNA binding (22, 23). The 14-3-3 protein recognition sites border the forkhead DNA binding domain; one is located at the N terminus and a second one at the wing W2 of FoxO-DBD. Because the wing W2 of FoxO-DBD might participate in DNA binding, it has been speculated that the interaction between the 14-3-3 protein and the wing W2 contributes to the inhibition of FoxO DNA-binding properties (24). To test whether this is also true in the case of FoxO4 we investigated the effect of the 14-3-3 protein binding on DNA-binding properties of intact FoxO4-DBD. First, the association of 14-3-3 protein (human isoform zeta) with phosphorylated FoxO4-DBD has been checked using native Tris borate-EDTA (TBE) buffer PAGE electrophoresis. As can be seen from Fig. 3*A*, the phosphorylated pFoxO4-DBD forms a stable complex with the 14-3-3 protein compared with unphosphorylated FoxO4-DBD (*e.g.* compare *lanes 4–6* and *7–9*). Formation of the stable 14-3-3 protein·pFoxO4-DBD complex was also confirmed using analytical gel filtration (data not shown). Next, we studied the effect of 14-3-3 protein binding on DNA-binding properties of FoxO4-DBD using fluorescence anisotropy-based binding assay (Fig. 3*B*). Titration data show that 14-3-3ζ protein can disrupt DNA complex of phosphorylated pFoxO4-DBD more efficiently compared with unphosphorylated FoxO4-DBD. The inhibitory effect of 14-3-3ζ protein, caused presumably by pFoxO4-DBD binding to the 14-3-3 protein, is consistent with similar observations made for *C. elegans* FoxO homologue DAF-16 and $dpFoxO4_{11-213}$ (22, 23). Partial dissociation of unphosphorylated FoxO4-DBD·DNA complex

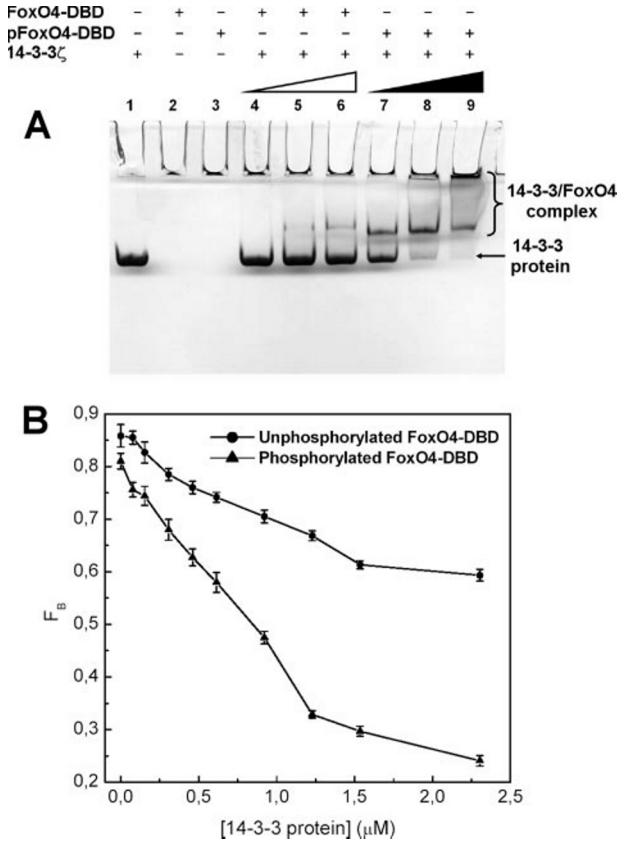

FIGURE 3. **The 14-3-3ζ protein interacts with pFoxO4-DBD phosphorylated by PKB at Ser[193].** *A*, native 12% TBE-PAGE electrophoresis with Coomassie Blue staining. 14-3-3 protein forms a stable complex with phosphorylated pFoxO4-DBD, whereas unphosphorylated FoxO4-DBD interacts with 14-3-3 protein very weakly. *Lane 1*, 14-3-3 protein (400 pmol); *lane 2*, FoxO4-DBD (400 pmol); *lane 3*, pFoxO4-DBD (400 pmol); *lanes 4–6*, titration of 14-3-3 protein (400 pmol) with unphosphorylated FoxO4-DBD (100, 250, and 400 pmol); *lanes 7–9*, titration of 14-3-3 protein with phosphorylated pFoxO4-DBD (100, 250, and 400 pmol). *B*, fluorescence anisotropy binding assay. 14-3-3ζ protein binding to phosphorylated pFoxO4-DBD inhibits DNA binding more efficiently compared with unphosphorylated FoxO4-DBD. Fluorescence anisotropy of dsDNA probe labeled with fluorescein was used to follow FoxO4-DBD·DNA complex dissociation. Concentration of FoxO4-DBD and dsDNA was 1400 nM and 100 nM, respectively.

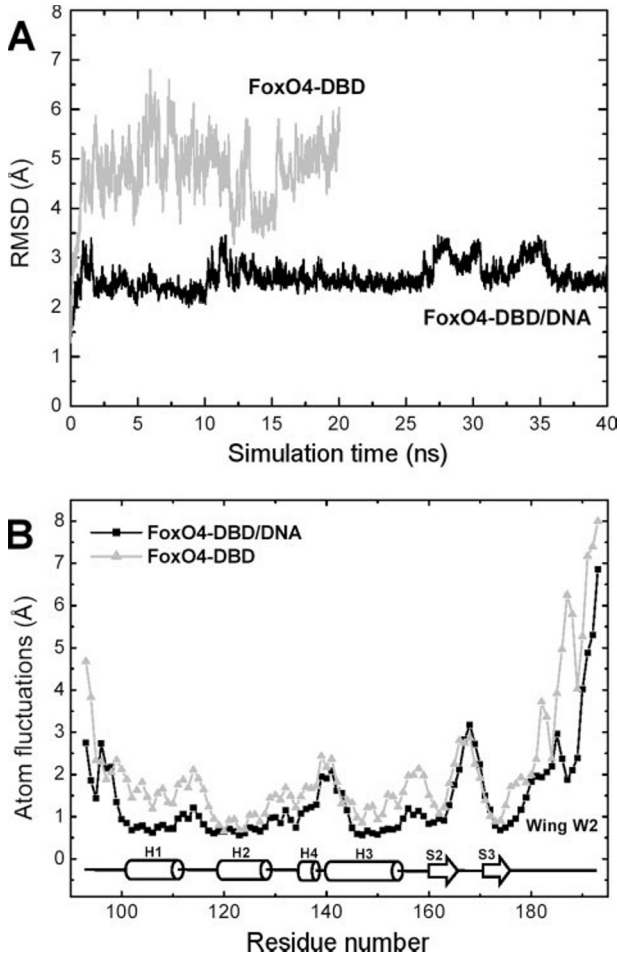

FIGURE 4. **Molecular dynamics simulation of free FoxO4-DBD and FoxO4-DBD·DNA complex.** *A*, time course of the r.m.s.d. values of the FoxO4-DBD backbone heavy atoms during production runs. *B*, the positional fluctuations of Cα atoms of both free FoxO4-DBD and its DNA-bound form. The wing W2 seems to be the most flexible region of FoxO4-DBD.

is probably caused by weak interaction between the 14-3-3ζ protein and FoxO4-DBD (Fig. 3*A*, *lanes 5* and *6*).

Molecular Dynamics Simulations of FoxO4-DBD·DNA Complex—Structures of HNF-3γ·DNA and Genesis·DNA complexes demonstrated that the wing W2 at the C terminus of forkhead domains of these transcription factors makes important contacts with DNA and helps stabilize the protein·DNA complex (5, 10). On the other hand, N-terminal extensions of these two forkhead domains do not interact with DNA as has been observed for forkhead transcription factors E2F4 and DP2 (12). Because no experimental structure of FoxO·DNA complex is available, it is unclear whether the same holds true for FoxO factors. Therefore, we performed molecular dynamics simulations of both free FoxO4-DBD (20 ns long) and its DNA-bound form (40 ns long) to both characterize conformational behavior of N- and C-terminal regions of FoxO4 forkhead domain and to generate a realistic model of FoxO4-DBD·DNA complex. The starting structure for MD simulations was prepared using the solution structure of FoxO4-DBD, and both the missing wing W2 and the position of canonical B-form DNA duplex were modeled using the HNF-3γ·DNA and Genesis·DNA structures as templates (5, 9, 10). The r.m.s.d. values of the protein backbone heavy atoms with respect to the starting structures are shown in Fig. 4*A*. Both simulations relaxed quickly from their initial conformation and remained stable over the simulated time. The r.m.s.d. values of the free FoxO4-DBD fluctuated around 4–6 Å, whereas those of the DNA-bound form are from 2 to 3 Å suggesting higher conformational flexibility of free FoxO4-DBD. The positional fluctuations of Cα atoms of both free FoxO4-DBD and its DNA-bound form are given in Fig. 4*B*. The positional displacements of residues 93–95 (N-terminal loop), 99–117 (helix H1), 152–161 (loop between H3 and S2), and 180–193 (wing W2) show marked differences between the free and DNA-bound forms. The wing W2 seems to be the most flexible region of FoxO4-DBD, and the suppression of its movements in the presence of DNA is likely the result of its contacts with the DNA.

Representative structures of both free FoxO4-DBD and its DNA-bound form were calculated as an average conformation of the most populated cluster obtained using a cluster analysis of simulated trajectories with a r.m.s.d. cutoff of 1.5 Å. The

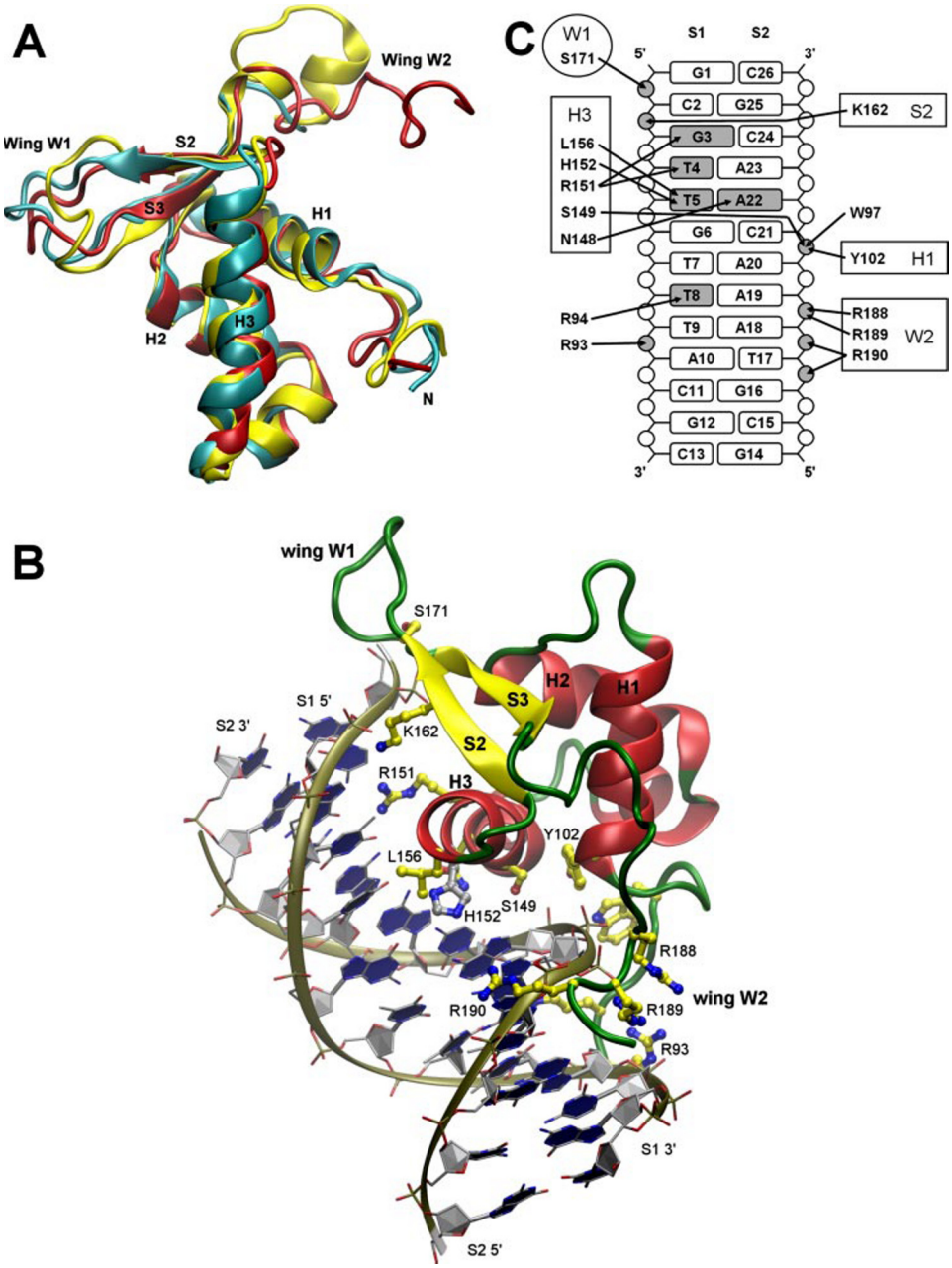

FIGURE 5. **Representative conformations of FoxO4-DBD and FoxO4-DBD·DNA complex.** *A*, the superimposition of representative conformations of free FoxO4-DBD (*yellow*) and FoxO4-DBD from DNA complex (*red*) with the solution structure of FoxO4-DBD (*cyan*) (9). Main-chain heavy atom r.m.s.d. values between the modeled and experimentally derived structures (with wing W2 excluded) were 2.15 Å for the free FoxO4-DBD and 2.35 Å for the DNA complex. *B*, representative structure of FoxO4-DBD·DNA complex. The regions of FoxO4-DBD predicted by MD simulation to be involved in contacts with DNA are the N-terminal loop (residues Arg^{93}, Arg^{94}, and Trp^{97}), helix H1 (Tyr^{102}), helix H3 (Asn^{148}, Ser^{149}, Arg^{151}, His^{152}, and Leu^{156}), strand S2 (Lys^{162}), wing W1 (Ser^{171}), and wing W2 (Arg^{188}, Arg^{189}, and Arg^{190}). *C*, schematic view of all predicted FoxO4-DBD-DNA contacts. Representative structures of both free FoxO4-DBD and its DNA-bound form were calculated as an average conformation of the most populated cluster obtained using a cluster analysis of simulated trajectories with an r.m.s.d. cutoff of 1.5 Å (45). This figure was generated using VMD (49).

superimposition of these representative conformations with solution structure of FoxO4-DBD is shown in Fig. 5*A*. Main-chain heavy atom r.m.s.d. values between the modeled and experimentally derived structures (with wing W2 excluded) were 2.15 Å for the free FoxO4-DBD and 2.35 Å for the DNA complex. Free FoxO4-DBD and its DNA complex significantly differ only in the conformation of the N-terminal loop and both wings. The rest of forkhead domain is relatively unchanged. The regions of FoxO4-DBD predicted by MD simulation to be involved in contacts with DNA are the N-terminal loop (residues Arg^{93}, Arg^{94}, and Trp^{97}), helix H1 (Tyr^{102}), helix H3 (Asn^{148}, Ser^{149}, Arg^{151}, His^{152}, and Leu^{156}), strand S2 (Lys^{162}), wing W1 (Ser^{171}), and wing W2 (Arg^{188}, Arg^{189}, and Arg^{190}) (Fig. 5, *B* and *C*). All these residues are highly conserved among FoxO transcription factors (Fig. 1*A*). Basic residues from wing W2 (Arg^{188}, Arg^{189}, and Arg^{190}) make contacts with phosphate groups of DNA backbone (Thr-17, Ala-18, and Ala-19 of strand S2). HNF-3γ and Genesis transcription factors make very similar contacts to the DNA, with exception of the N-terminal loop upstream of α-helix H1 (5, 10). This region, however, was found to interact with DNA in co-crystal structures of winged helix proteins E2F4 and DP2 (12). Simulation also suggests that FoxO4-DBD deforms DNA molecule by inducing a 19° bend.

Investigation of the Wing W2 Location Using FRET—FRET measurements between AEDANS moiety attached at two different positions within the wing W2 and a fluorescein moiety attached at 5′-end of either the sense or the antisense strand of dsDNA were used to investigate interaction between the wing W2 at the C terminus of forkhead domain and DNA. To specifically label the wing W2 for FRET measurements, we have constructed two FoxO4-DBD mutants containing a single Cys residue located at two different positions within the wing W2: Cys^{183} (this mutant was named FoxO4-DBDc183) and Cys^{193} (FoxO4-DBDc193). These two sites border the cluster of positively charged residues ($Arg^{188-190}$) that are potentially involved in DNA binding (Fig. 1*B*). The Cys residues were selectively labeled with the extrinsic fluorophore 1,5-IAEDANS as energy donor. Labeling experiments revealed that both FoxO4-DBD mutants can be completely modified by 1,5-IAEDANS. The stoichiometries of AEDANS/mol of these two FoxO4-DBD mutants were found to be ~1. The DNA binding abilities of both unlabeled and labeled

FoxO4-DBD mutants were checked using the electrophoretic mobility shift assay, and no significant differences were found (data not shown).

The presence of the energy transfer between AEDANS moiety attached to a cysteine residue of FoxO4-DBD and fluorescein moiety bound to the 5′-end of dsDNA was tested using the steady-state fluorescence. Fluorescence emission spectra of AEDANS-labeled FoxO4-DBD in the absence (both strands of dsDNA were unlabeled) and presence of fluorescein-labeled dsDNA (either the sense or antisense strand of dsDNA was labeled) are shown in Fig. 6. When excited at 336 nm, the AEDANS group has a fluorescence emission maximum near 488 nm. In the presence of fluorescein-labeled dsDNA the donor steady-state fluorescence intensities of both FoxO4-DBD mutants were quenched by ~30–40% compared with proteins with bound unlabeled dsDNA, indicating the presence of FRET. The sensitized fluorescence emission of fluorescein (induced by the nonradiative energy transfer from AEDANS group) was observed as a peak at 521 nm.

Time-resolved fluorescence intensities of AEDANS-labeled FoxO4-DBD mutants exhibited complex fluorescence decays. The time-resolved emission data were analyzed by the singular value decomposition maximum entropy method and mean excited-state lifetimes (τ_{mean}) were calculated as described previously (35). Lifetimes of AEDANS in the absence and in the presence of acceptor as well as efficiencies of the energy transfer are presented in Table 1. In the presence of fluorescein-labeled dsDNA for both FoxO4-DBD mutants the τ_{mean} of donor was reduced as a result of the energy transfer (Fig. 7). Values of the FRET efficiency were used to calculate the average distances between the donor-acceptor pair. Distances between AEDANS moiety attached to Cys^{183} or Cys^{193} of FoxO4-DB and fluorescein attached to the 5′-end of either sense or antisense strand of dsDNA were calculated to be in range from 56.4 to 62.3 Å (Table 1).

To compare results of molecular dynamics simulation with FRET measurements the time evolution of distances between atoms corresponding to AEDANS and fluorescein attachment sites were calculated (Fig. 8*A*). Distances between residue Ser^{183} and 5′-ends of both strands were relatively constant throughout the production run with average distance of 33.5 ± 1.5 Å for pair Ser^{183}–G1 (strand S1) and 36.5 ± 2.9 Å for Ser^{183}–G14 (strand S2). On the other hand, distances between residue Ser^{193} and 5′-ends of both strands substantially fluctuated with average distance of 39.2 ± 5.4 Å for pair Ser^{193}–G1 (strand S1) and 22 ± 6.3 Å for Ser^{193}–G14 (strand S2). These fluctuations can be explained by the high flexibility of the C terminus of wing W2 in agreement with high positional fluctuations of its Cα atoms (Fig. 6*B*). If we consider both the most probable position of the fluorescein moiety at the 5′-end of DNA duplex (46, 47) and the size of dansyl moiety, the three of four calculated distances are consistent with our FRET measurements (Fig. 8*B* and Table 1). The fourth distance between AEDANS attached at residue 193 and fluorescein at 5′-end of S2 strand is shorter by ~8 Å compared with the distance determined by FRET. Our simulated system does not contain fluorescein nor AEDANS moiety, and repulsion between negatively charged AEDANS and DNA in FRET experiments might keep Cys^{193}-AEDANS further away from the DNA compared with the simulation. However, both experimental distances involving Cys^{193}-AEDANS and 5′-ends of both strands can be satisfied by a small conformational change of the very C terminus of wing W2 (residues Arg^{190}–Ser^{193}) while keeping residues Arg^{188} and Arg^{189} still interacting with the DNA.

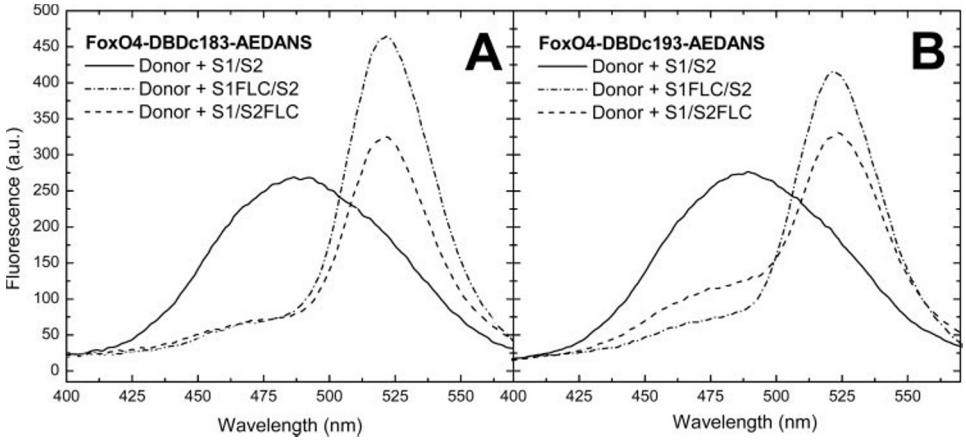

FIGURE 6. **Steady-state fluorescence emission spectra of energy donor AEDANS attached at Cys^{183} or Cys^{193} of FoxO4-DBD and acceptor fluorescein attached at the 5′-end of one strand of dsDNA.** Donor only spectra (*solid line*) and donor-acceptor FoxO4-DBD·DNA complexes spectra (*dotted* and *dashed lines*) are shown for the FoxO4-DBDc183 mutant (*A*) and the FoxO4-DBDc193 mutant (*B*).

Taken together, both FRET measurements and MD simulation suggest that the wing W2 of FoxO4-

TABLE 1
Summary of Förster energy transfer measurements

FoxO4-DBD mutant	Label	dsDNA	τ_{mean}[a]	E[b]	R[c]	D[d]
			ns	*%*	*Å*	
FoxO4-DBDc183	AEDANS only	S1/S2	14.85			
FoxO4-DBDc183	AEDANS + fluorescein	S1FLC/S2	10.37	30.2	56.4	56
FoxO4-DBDc183	AEDANS + fluorescein	S1/S2FLC	11.88	20.0	61.7	62
FoxO4-DBDc193	AEDANS only	S1/S2	15.25			
FoxO4-DBDc193	AEDANS + fluorescein	S1FLC/S2	11.58	24.1	59.3	60
FoxO4-DBDc193	AEDANS + fluorescein	S1/S2FLC	12.34	19.1	62.3	54

[a] Mean lifetimes were calculated as $\tau_{mean} = \Sigma_i f_i \tau_i$, where f_i is an intensity fraction of the ith lifetime component τ_i.
[b] E, energy transfer efficiency.
[c] R, distance between donor-acceptor pair calculated as $R = R_0\sqrt[6]{1/E - 1}$, where R_0 is the Förster critical distance. An R_0 value of 49 Å was used to calculate R (36, 37).
[d] D, distance between donor-acceptor pair estimated from MD simulation.

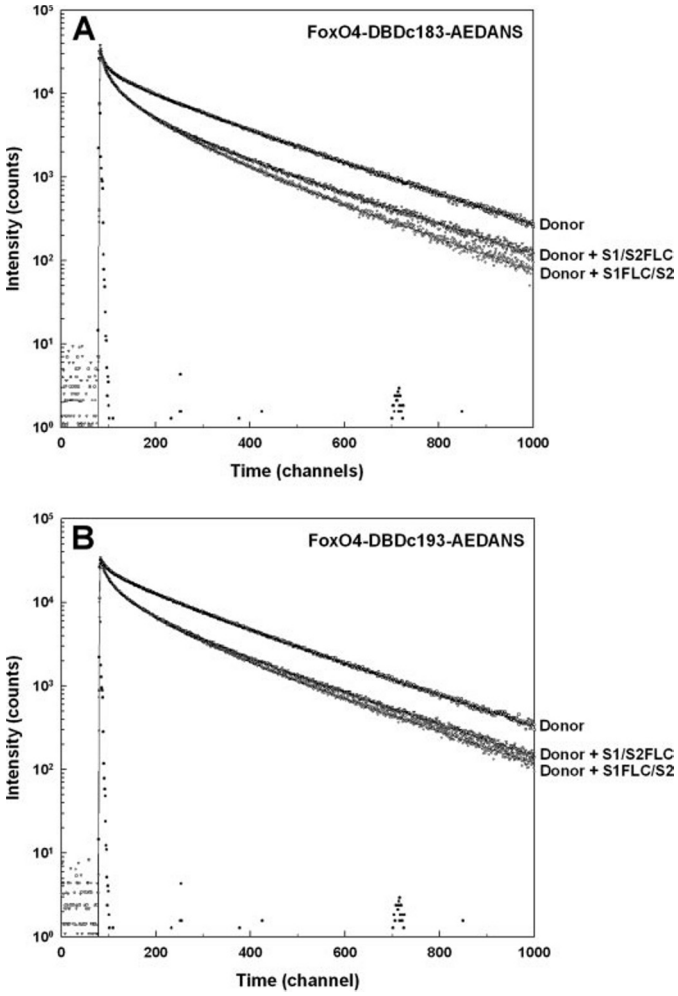

FIGURE 7. **Fluorescence energy transfer in FoxO4-DBD·DNA complexes.** Comparison of fluorescence decays of AEDANS attached at Cys^{183} (*A*) or Cys^{193} (*B*) of FoxO4-DBD in the absence (*open squares*, unlabeled dsDNA S1/S2 was used) and in the presence (*triangles* and *open circles*) of fluorescein-labeled dsDNA (S1FLC/S2 or S1/S2FLC). The calibration is 73 ps/channel.

DBD interacts with DNA in similar fashion as shown for transcription factors HNF-3γ and Genesis (5, 10).

DISCUSSION

The DNA binding domain of forkhead box transcription factors is a compact α/β structure containing a classic helix-turn-helix DNA binding motif within a three-helix bundle, braced against an antiparallel β-sheet (4, 5, 7–11). In addition, an extended loop between β-strands and the loop C-terminal to the β-sheet create two wing-like structures (Fig. 1*A*). The main DNA binding portion of forkhead box DBD is the H3 recognition helix. Other regions of forkhead domain that can make important interactions with DNA are wings (5) or N-terminal extension upstream of helix H1 (12). The likely function of these regions is the stabilization of protein·DNA complex.

Interaction of N-terminal Loop and Wing W2 of FoxO4-DBD with DNA—In the FoxO subset of Fox proteins the wing W2 contains a 14-3-3 protein-binding motif that is phosphorylated by PKB in response to insulin or growth factors (18, 23, 24, 26). Both PKB-induced phosphorylation and the 14-3-3 protein binding have been suggested to reduce the DNA-binding potential of FoxO factors, and the alteration of wing W2 structure can be one of the main reasons of this inhibition (22–24, 28, 30). Structures of forkhead transcription factors HNF-3γ and Genesis with bound DNA revealed that wing W2 participates in DNA binding through a cluster of basic residues (5, 10). If the same is true for FoxO4-DBD then it could explain the inhibitory effect of the 14-3-3 protein on its DNA-binding properties. The cluster of basic residues at the C-terminal end of wing W2 is an integral part of 14-3-3 protein-binding motif, and upon the 14-3-3 protein binding it would be buried within the 14-3-3 protein ligand binding groove and unable to interact with DNA (48). To test whether the wing W2 of FoxO4-DBD is directly involved in DNA binding, we first prepared a C-terminally truncated version of FoxO4-DBD missing the wing W2. The truncation of wing W2 caused only a 2-fold decrease in DNA binding affinity (Fig. 2). This result contrasts with the observation that removal of basic residues from wing W2 of closely related FoxO1-DBD completely inhibits its binding to the DNA (28). However, the construct used in our experiments contains the N-terminal loop upstream of helix H1 (residues Arg^{82}–Ala^{96} in the FoxO4 sequence), whereas FoxO1-DBD used by Zhang *et al.* (28) does not. To create a comparable construct of FoxO4-DBD we removed this N-terminal extension and observed a decrease in DNA binding affinity of ~2-fold compared with intact DBD. Upon the additional removal of wing W2 the DNA-binding potential of FoxO4-DBDΔNΔC was significantly inhibited as in the case of C-terminally truncated FoxO1-DBD used by Zhang *et al.* (28). Therefore, it seems that both N-terminal extension and C-terminal wing W2 are important for the stability of FoxO-DBD·DNA complex.

Because no experimental structure of FoxO-DBD with bound DNA is available we used molecular dynamics simulations and FRET measurements to investigate the conformation of N-terminal loop and wing W2 of FoxO4-DBD and their interactions with DNA. Our results suggest that both regions make contacts with DNA in agreement with the binding experiments. MD simulations predict that three residues from the N-terminal loop (Arg^{93}, Arg^{94}, and Trp^{97}) interact with DNA (Fig. 5*C*). Similar contacts between positively charged residues from this region DBD and DNA have been observed in co-crystal structure of forkhead transcription factors E2F4 and DP2 (12). MD simulations together with FRET measurements indicate that basic residues within the wing W2 (Arg^{188} and Arg^{189}) interact with DNA in a similar fashion as shown for transcription factors HNF-3γ and Genesis (Figs. 5*B*, 5*C*, 8*A*, and 8*B*) (5, 10).

Effect of Phosphorylation and 14-3-3 Protein Binding—Phosphorylation of the second PKB/14-3-3 binding motif at the wing W2 of DBD has been shown to suppress DNA binding of FoxO1 and FoxO6 factors (28, 30). On the other hand, PKB-mediated phosphorylation of both DAF-16 (*C. elegans* FoxO homologue) and FoxO4 (fragment 11–213) does not by itself affect their DNA binding abilities, and the association with the 14-3-3 protein has been shown to be necessary for complete inhibition of DNA binding (22, 23). Our binding experiments revealed that PKB-induced phosphorylation of Ser^{193} has a negligible effect on DNA binding affinity of intact FoxO4-DBD

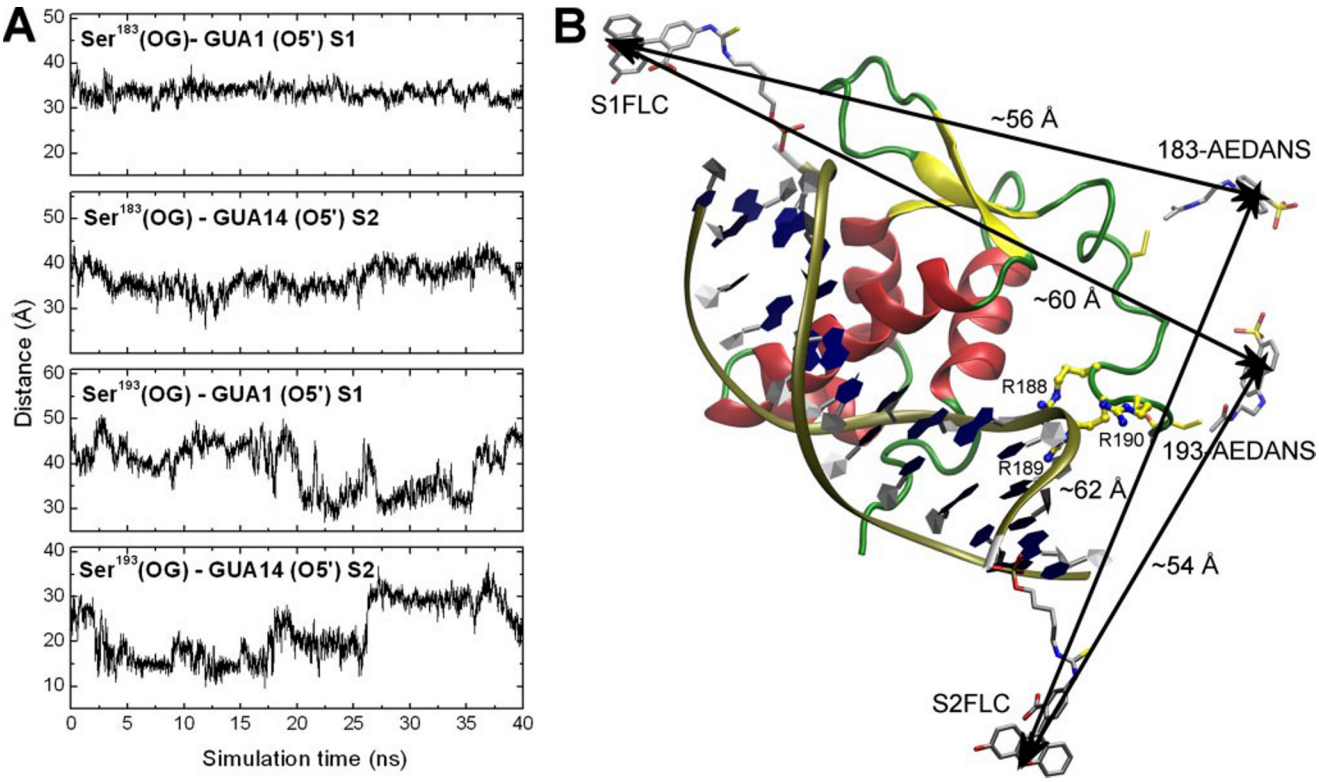

FIGURE 8. **Comparison of molecular dynamics simulation with FRET measurements.** *A*, the time evolution of distances between atoms corresponding to AEDANS and fluorescein attachment sites. Distances between residue Ser^{183} and 5′-ends of both strands were relatively constant during the whole simulation with average distances of 33.5 ± 1.5 Å for pair Ser^{183}–G1 (strand S1) and 36.5 ± 2.9 Å for Ser^{183}–G14 (strand S2). Distances between residue Ser^{193} and 5′-ends of both strands substantially fluctuated with average distance of 39.2 ± 5.4 Å for pair Ser^{193}–G1 (strand S1) and 22 ± 6.3 Å for Ser^{193}–G14 (strand S2). *B*, distances between AEDANS and fluorescein moieties estimated from MD simulation. If we consider both the most probable position of the fluorescein moiety at the 5′-end of DNA duplex (46, 47) and the size of dansyl moiety, three of four calculated distances are consistent with our FRET measurements (Table 1). The fourth distance between AEDANS attached at residue 193 and fluorescein at 5′-end of S2 strand is shorter by ~8 Å compared with the distance determined by FRET. However, both experimental distances involving Cys^{193}-AEDANS and 5′-ends of both strands can be satisfied by a small conformational change of the very C terminus of wing W2 (residues Arg^{190}–Ser^{193}) while keeping residues Arg^{188} and Arg^{189} still interacting with the DNA. This figure was generated using VMD (49).

(Fig. 2) in agreement with our previous observations that PKB-induced phosphorylation had no significant effect on DNA binding of FoxO4$_{11-213}$ (23, 27). A possible explanation for the observed differences between FoxO1-DBD and FoxO4-DBD might be again in the absence of the N-terminal loop in FoxO1-DBD construct used by Zhang *et al.* (28). When we phosphorylated N-terminally truncated FoxO4-DBDΔN (comparable to the FoxO1-DBD construct used in Ref. 28), we have observed strong inhibition of DNA-binding potential (Fig. 2).

Our results indicate that the introduction of negative charge by itself cannot be the only factor inhibiting the DNA-binding potential of intact FoxO4-DBD. Phosphorylation of Ser^{193} might inhibit DNA binding of FoxO4 indirectly through the binding of 14-3-3 protein. Titration data show that the 14-3-3 protein binding to phosphorylated wing W2 of FoxO4-DBD can efficiently dissociate the FoxO4-DBD·DNA complex, whereas in the absence of phosphorylation the inhibitory effect of 14-3-3 protein is significantly weaker (Fig. 3*B*). Because the removal of wing W2 does not have as strong an inhibitory effect on FoxO4-DBD binding to the DNA, the inhibition caused by 14-3-3 protein likely arises not only from the interaction between 14-3-3 and wing W2 but potentially also from interactions with other region(s) of the forkhead domain.

In conclusion, our results show that both N-terminal loop located upstream of helix H1 and C-terminal wing W2 are important for FoxO4-DBD binding to the DNA. Although the removal of either region results in partial reduction of DNA binding, the simultaneous deletion of both portions inhibits DNA binding significantly. The PKB-induced phosphorylation of wing W2 by itself has negligible effect on DNA binding, whereas the complex formation between 14-3-3 protein and phosphorylated FoxO4-DBD inhibits DNA binding efficiently.

REFERENCES

1. Kaufmann, E., and Knochel, W. (1996) *Mech. Dev.* **57,** 3–20
2. Lai, E., Clark, K. L., Burley, S. K., and Darnell, J. E., Jr. (1993) *Proc. Natl. Acad. Sci. U. S. A.* **90,** 10421–10423
3. Carlsson, P., and Mahlapuu, M. (2002) *Dev. Biol.* **250,** 1–23
4. Kaestner, K. H., Knochel, W., and Martinez, D. E. (2000) *Genes Dev.* **14,** 142–146
5. Clark, K. L., Halay, E. D., Lai, E., and Burley, S. K. (1993) *Nature* **364,** 412–420
6. Jin, C., and Liao, X. (1999) *J. Mol. Biol.* **292,** 641–651
7. Gajiwala, K. S., and Burley, S. K. (2000) *Curr. Opin. Struct. Biol.* **10,** 110–116
8. Gajiwala, K. S., Chen, H., Cornille, F., Roques, B. P., Reith, W., Mach, B., and Burley, S. K. (2000) *Nature* **403,** 916–921
9. Weigelt, J., Climent, I., Dahlman-Wright, K., and Wikstrom, M. (2001) *Biochemistry* **40,** 5861–5869
10. Jin, C., Marsden, I., Chen, X., and Liao, X. (1999) *J. Mol. Biol.* **289,** 683–690
11. Wolberger, C., and Campbell, R. (2000) *Nat. Struct. Biol.* **7,** 261–262
12. Zheng, N., Fraenkel, E., Pabo, C. O., and Pavletich, N. P. (1999) *Genes Dev.* **13,** 666–674

13. Pierrou, S., Hellqvist, M., Samuelsson, L., Enerback, S., and Carlsson, P. (1994) *EMBO J.* **13,** 5002–5012
14. van Dongen, M. J., Cederberg, A., Carlsson, P., Enerback, S., and Wikstrom, M. (2000) *J. Mol. Biol.* **296,** 351–359
15. Arden, K. C. (2004) *Mol. Cell* **14,** 416–418
16. Burgering, B. M., and Kops, G. J. (2002) *Trends Biochem. Sci.* **27,** 352–360
17. Van Der Heide, L. P., Hoekman, M. F., and Smidt, M. P. (2004) *Biochem. J.* **380,** 297–309
18. Brunet, A., Bonni, A., Zigmond, M. J., Lin, M. Z., Juo, P., Hu, L. S., Anderson, M. J., Arden, K. C., Blenis, J., and Greenberg, M. E. (1999) *Cell* **96,** 857–868
19. Woods, Y. L., and Rena, G. (2002) *Biochem. Soc. Trans.* **30,** 391–397
20. Woods, Y. L., Rena, G., Morrice, N., Barthel, A., Becker, W., Guo, S., Unterman, T. G., and Cohen, P. (2001) *Biochem. J.* **355,** 597–607
21. Rena, G., Woods, Y. L., Prescott, A. R., Peggie, M., Unterman, T. G., Williams, M. R., and Cohen, P. (2002) *EMBO J.* **21,** 2263–2271
22. Cahill, C. M., Tzivion, G., Nasrin, N., Ogg, S., Dore, J., Ruvkun, G., and Alexander-Bridges, M. (2001) *J. Biol. Chem.* **276,** 13402–13410
23. Obsil, T., Ghirlando, R., Anderson, D. E., Hickman, A. B., and Dyda, F. (2003) *Biochemistry* **42,** 15264–15272
24. Zhao, X., Gan, L., Pan, H., Kan, D., Majeski, M., Adam, S. A., and Unterman, T. G. (2004) *Biochem. J.* **378,** 839–849
25. Brownawell, A. M., Kops, G. J., Macara, I. G., and Burgering, B. M. (2001) *Mol. Cell. Biol.* **21,** 3534–3546
26. Brunet, A., Kanai, F., Stehn, J., Xu, J., Sarbassova, D., Frangioni, J. V., Dalal, S. N., DeCaprio, J. A., Greenberg, M. E., and Yaffe, M. B. (2002) *J. Cell Biol.* **156,** 817–828
27. Obsilova, V., Vecer, J., Herman, P., Pabianova, A., Sulc, M., Teisinger, J., Boura, E., and Obsil, T. (2005) *Biochemistry* **44,** 11608–11617
28. Zhang, X., Gan, L., Pan, H., Guo, S., He, X., Olson, S. T., Mesecar, A., Adam, S., and Unterman, T. G. (2002) *J. Biol. Chem.* **277,** 45276–45284
29. Lai, E., Prezioso, V. R., Smith, E., Litvin, O., Costa, R. H., and Darnell, J. E., Jr. (1990) *Genes Dev.* **4,** 1427–1436
30. van der Heide, L. P., Jacobs, F. M., Burbach, J. P., Hoekman, M. F., and Smidt, M. P. (2005) *Biochem. J.* **391,** 623–629
31. Kovarova, H., Halada, P., Man, P., Golovliov, I., Krocova, Z., Spacek, J., Porkertova, S., and Necasova, R. (2002) *Proteomics* **2,** 85–93
32. Silhan, J., Obsilova, V., Vecer, J., Herman, P., Sulc, M., Teisinger, J., and Obsil, T. (2004) *J. Biol. Chem.* **279,** 49113–49119
33. Obsil, T., Ghirlando, R., Klein, D. C., Ganguly, S., and Dyda, F. (2001) *Cell* **105,** 257–267
34. Kohler, J. J., and Schepartz, A. (2001) *Biochemistry* **40,** 130–142
35. Obsilova, V., Herman, P., Vecer, J., Sulc, M., Teisinger, J., and Obsil, T. (2004) *J. Biol. Chem.* **279,** 4531–4540
36. Squier, T. C., Bigelow, D. J., Deancos, J. G., and Inesi, G. (1987) *J. Biol. Chem.* **262,** 4748–4754
37. Birmachu, W., Nisswandt, F. L., and Thomas, D. D. (1989) *Biochemistry* **28,** 3940–3947
38. Sorin, E. J., and Pande, V. S. (2005) *Biophys. J.* **88,** 2472–2493
39. Lu, X. J., and Olson, W. K. (2003) *Nucleic Acids Res.* **31,** 5108–5121
40. Jorgensen, W. L., Chandrasekhar, J., Madura, J. D., Impey, R. W., and Klein, M. L. (1983) *J. Chem. Phys.* **79,** 926–935
41. Berendsen, H. J. C., Postma, J. P. M., Vangunsteren, W. F., Dinola, A., and Haak, J. R. (1984) *J. Chem. Phys.* **81,** 3684–3690
42. Hess, B., Bekker, H., Berendsen, H. J. C., and Fraaije, J. G. E. M. (1997) *J. Comput. Chem.* **18,** 1463–1472
43. Darden, T., York, D., and Pedersen, L. (1993) *J. Chem. Phys.* **98,** 10089–10092
44. Van der Spoel, D., Lindahl, E., Hess, B., Groenhof, G., Mark, A. E., and Berendsen, H. J. C. (2005) *J. Comput. Chem.* **26,** 1701–1718
45. Daura, X., Gademann, K., Jaun, B., Seebach, D., van Gunsteren, W. F., and Mark, A. E. (1999) *Angew. Chem. Int. Ed. Engl.* **38,** 236–240
46. Norman, D. G., Grainger, R. J., Uhrin, D., and Lilley, D. M. (2000) *Biochemistry* **39,** 6317–6324
47. Clegg, R. M., Murchie, A. I., Zechel, A., and Lilley, D. M. (1993) *Proc. Natl. Acad. Sci. U. S. A.* **90,** 2994–2998
48. Yaffe, M. B., Rittinger, K., Volinia, S., Caron, P. R., Aitken, A., Leffers, H., Gamblin, S. J., Smerdon, S. J., and Cantley, L. C. (1997) *Cell* **91,** 961–971
49. Humphrey, W., Dalke, A., and Schulten, K. (1996) *J. Mol. Graphics* **14,** 33-8, 27-8